*Progress In Electromagnetics Research C, Vol. 131, 227–240, 2023*

# Effects of Defect Layers and Loss Factors on Transmission Spectrum for One-Dimensional Lossy Metamaterial Photonic Crystal

**Rawdha Thabet*, Ouarda Barkat, and Mohamed L. Riabi**

**Abstract**—An exhaustive numerical analysis is presented on the effects of defect layers and electric and magnetic loss factors on the transmission spectrum of one-dimensional metamaterial photonic crystal. The proposed structure is a symmetrical multilayer configuration consisting of alternating layers of lossy metamaterial and double-positive material, with a defective region in the middle. The study shows that one or more defect transmission modes are generated in photonic band gaps. The optical properties have been numerically analyzed and simulated using the transfer matrix method. Parameters, such as permittivity, thickness, and number of defect layers, influence the band gap width and the tunability of the defect peak frequency. The effects of the electric and magnetic loss factors (or damping frequencies) of the metamaterial on the intensity and on the quality factor of the defect modes are also well observed. The analysis is validated by comparing the results to some available in the literature, and the proposed structure can be exploited in the design of narrowband filters in the microwave domain.

## 1. INTRODUCTION

Artificial structures, such as photonic crystals, have been extensively studied in recent years due to their prominent physical and optical properties [1–3]. These structures employ periodic cellular units. Photonic crystals, containing metamaterial, are currently among the most widely used in engineering applications for microwave and terahertz frequencies, due to the enhancement that this material provides to the properties of photonic crystals [4]. This kind of structures has already led to remarkable achievements and still allows researchers to consider further scientific and technological advancements [5–8].

Metamaterials are the subject of great interest in the electromagnetic community [9–12]. They are artificial structural elements, composed of sets of microscopic resonators acting collectively to imitate a homogeneous medium with electromagnetic properties that exceed those found in nature [13]; one has to look for strong spectral resonances of the permittivity $\epsilon$ and permeability $\mu$ [14]. They can exhibit simultaneous negative permittivity and permeability and are called, in this case, double-negative (DNG) materials. These properties are described using the Lorentz and Drude medium models [15–21]. Models that are the most popular in electromagnetic metamaterial simulations and that involve parameters include the electric and magnetic damping frequencies (or what are called electric and magnetic loss factors). The permittivity and permeability present complex values whose imaginary parts reflect losses.

The one-dimensional photonic crystal (1DPC) consists of a periodic alternation of layers of materials with different refractive indices [22, 23]. This configuration makes it possible to obtain photonic band gaps (PBGs); frequency ranges over which electromagnetic waves are forbidden [24]. The spatial periodicity can be broken when layers of defects are created in the 1DPC structure allowing, thus, the generation of what are called modes of defects (or transmission modes) within the PBG [25].

*Received 14 January 2023, Accepted 21 March 2023, Scheduled 30 March 2023*

* Corresponding author: Rawdha Thabet (rawdha.thabet@umc.edu.dz).

The authors are with the Laboratory of Electromagnetism and Telecommunications, Department of Electronics, University Mentouri-Constantine 1, Constantine 25000, Algeria.

One-dimensional metamaterial photonic crystals (1DMPCs), which are 1DPC achieving periodicity by integrating layers of metamaterial, are structures on a sub-wavelength scale. Such structures appear homogeneous for optical fields, and the resulting remarkable properties are explained essentially by unusual values of the refractive index [8, 26–28]. In a 1DMPC structure, the light could be controlled, on the wavelength scale, by a periodic modulation of $\epsilon$ and $\mu$, resulting in complex Bragg reflections. A good alternative to this approach could be to have direct control over the spectral dispersion of $\epsilon(w)$ and $\mu(w)$. The applications of 1DMPC are in different fields, including optical filters, optical hyper lens, invisible cloaking, lenses for high-gain antennas and laser applications.

In this paper, a defective symmetric 1DMPC integrating DNG material layers and defect layers in the middle of the structure are treated. The transmission spectra are obtained using the transfer matrix method (TMM) [29–32] and are presented for two successive PBGs. The ability of tuning the transmission peak frequency of defect mode and the number of these modes in the PBG is investigated by varying parameters such as thickness, permittivity of defect layers, and number of these defect layers. The effects of electric and magnetic loss factors, on the frequency behavior of the defect mode, are also highlighted. They are examined in terms of transmission efficiency and quality factor. The numerical results are provided using Matlab, and the accuracy of the analysis is tested by comparing some computed results with published data.

## 2. THEORETICAL MODEL

We present, in Figure 1, the geometric model proposed for study. It is a 1DMPC formed by alternating layers of a lossy metamaterial $A$ and a double-positive (DPS) material $B$. The structure is symmetric and configured in the form $Air/(AB)^{N/2}/D/(BA)^{N/2}/Air$. Defect region $D$ composed of three ($N_d = 3$) layers $D_1$, $D_2$, $D_1$, of thicknesses $d_{f_1}$, $d_{f_2}$, $d_{f_1}$ and permittivities $\epsilon_{f_1}$, $\epsilon_{f_2}$, $\epsilon_{f_1}$, is placed at the middle of the design structure. The layers $A$ and $B$ have, respectively, thicknesses $d_A$ and $d_B$, permittivities $\epsilon_A$ and $\epsilon_B$. $N$ is the periodicity number. $d = d_A + d_B$ is the spatial period.

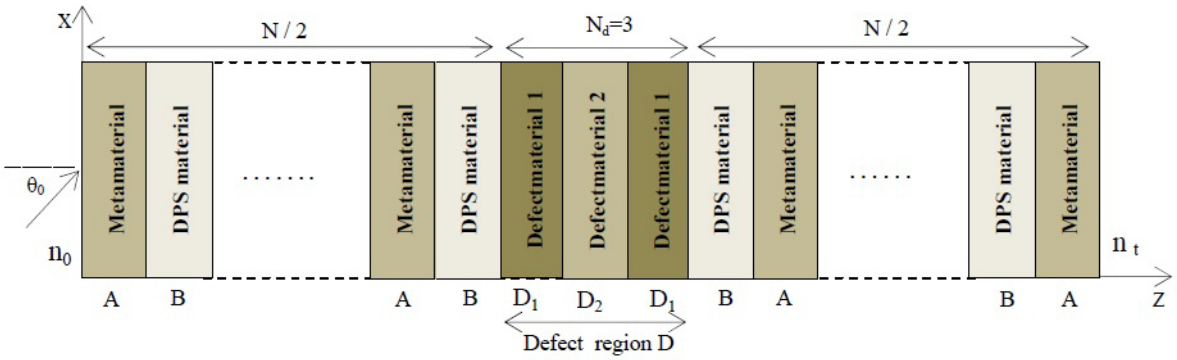


**Figure 1.** Schematic diagram of the defective 1DMPC structure composed of alternating metamaterial and DPS layers with $N_d = 3$ defective layers in the middle.

Based on the Maxwell equations and boundary conditions, the well-known TMM has been widely used to determine the amplitude and phase spectra of the light wave propagating in such structures. The components of the electric $\vec{E}$ and magnetic $\vec{H}$ fields in the $j$th layer, for propagation according to the $xoz$ plane and a TM ($p$) polarization, can be written as [30, 33]:

$$H_{jy} = A_j^{(p)} e^{i(wt - k_j(z\cdot\cos\theta_j + x\cdot\sin\theta_j))} + B_j^{(p)} e^{i(wt + k_j(z\cdot\cos\theta_j - x\cdot\sin\theta_j))} \quad (1)$$

$$E_{jx} = \eta_j \cos\theta_j \left( A_j^{(p)} e^{i(wt - k_j(z\cdot\cos\theta_j + x\cdot\sin\theta_j))} - B_j^{(p)} e^{i(wt + k_j(z\cdot\cos\theta_j - x\cdot\sin\theta_j))} \right) \quad (2)$$

$$E_{jz} = -\eta_j \sin\theta_j \left( A_j^{(p)} e^{i(wt - k_j(z\cdot\cos\theta_j + x\cdot\sin\theta_j))} + B_j^{(p)} e^{i(wt + k_j(z\cdot\cos\theta_j - x\cdot\sin\theta_j))} \right) \quad (3)$$

The components of the $\vec{E}$ and $\vec{H}$ fields in the $j$th layer, for TE ($s$) polarization, are given by:

$$E_{jy} = A_j^{(s)} e^{i(wt - k_j(z\cdot\cos\theta_j + x\cdot\sin\theta_j))} + B_j^{(s)} e^{i(wt + k_j(z\cdot\cos\theta_j - x\cdot\sin\theta_j))} \tag{4}$$

$$H_{jx} = -\frac{\cos\theta_j}{\eta_j}\left(A_j^{(s)} e^{i(wt - k_j(z\cdot\cos\theta_j + x\cdot\sin\theta_j))} - B_j^{(s)} e^{i(wt + k_j(z\cdot\cos\theta_j - x\cdot\sin\theta_j))}\right) \tag{5}$$

$$H_{jz} = \frac{\sin\theta_j}{\eta_j}\left(A_j^{(s)} e^{i(wt - k_j(z\cdot\cos\theta_j + x\cdot\sin\theta_j))} + B_j^{(s)} e^{i(wt + k_j(z\cdot\cos\theta_j - x\cdot\sin\theta_j))}\right) \tag{6}$$

$A_j^{(p)(\text{or }(s))}$ and $B_j^{(p)(\text{or }(s))}$ are the field amplitudes for the forward and backward travelling waves in the $j$th layer. $k_j$ is the wave number, and $\eta_j$ is the intrinsic impedance, such that:

$$k_j = w\sqrt{\epsilon_0\mu_0\epsilon_j\mu_j} \tag{7}$$

$$\eta_j = \frac{k_j}{w\epsilon_0\epsilon_j} = \sqrt{\frac{\mu_0\mu_j}{\epsilon_0\epsilon_j}} \tag{8}$$

$w$ is the angular frequency of incident wave. $\epsilon_0$ and $\mu_0$ are the permittivity and permeability in vacuum. $\epsilon_j$, $\mu_j$, and $\theta_j$ are, respectively, the relative permittivity, relative permeability, and ray angle in the $j$th layer of refractive index $n_j = \sqrt{\epsilon_j\mu_j}$.

By using the continuity conditions for $\vec{E}$ field at the different interfaces ($z = 0$, $z = d_A$, $z = d_A + d_B$, $z = 2d_A + d_B$, .....), the transmittance matrix $M$ of the entire structure can be constructed. For a 1DPC structure consisting of $N$ layers, this matrix is given by [29, 30, 34–36]:

$$\begin{pmatrix} E_t \\ H_t \end{pmatrix} = M \begin{pmatrix} E_0 \\ H_0 \end{pmatrix} \tag{9}$$

where

$$M = \prod_{j=1}^{N} M_j = \begin{pmatrix} M_{11} & M_{12} \\ M_{21} & M_{22} \end{pmatrix} \tag{10}$$

$E_0$, $H_0$ are the incident electric and magnetic fields, and $E_t$, $H_t$ are the electric and magnetic fields in the last medium. $M_{11}$, $M_{12}$, $M_{21}$, and $M_{22}$ are the elements of the total transmittance matrix, and $M_j$ is the characteristic matrix of the $j$th layer, which can be written in the form:

$$M_j = \begin{pmatrix} \cos(\delta_j) & \frac{1}{iq_j}\sin(\delta_j) \\ -iq_j\sin(\delta_j) & \cos(\delta_j) \end{pmatrix} \tag{11}$$

$\delta_j$ and $q_j$ are the matrix parameters. They are expressed as:

$$\delta_j = k_j d_j \cos\theta_j = \frac{w}{c} n_j d_j \cos\theta_j \tag{12}$$

and

$$q_j = \begin{cases} \sqrt{\dfrac{\epsilon_j}{\mu_j}}\cos\theta_j & \text{for TE mode} \\ \sqrt{\dfrac{\mu_j}{\epsilon_j}}\cos\theta_j & \text{for TM mode} \end{cases} \tag{13}$$

with $d_j$ the thickness of layer $j$ and $c$ the speed of light. We note also that $\theta_j$ is related to the angle of incidence of light $\theta_0$ by the Snell-Descartes law:

$$n_j\sin\theta_j = n_0\sin\theta_0 \tag{14}$$

For the case of the structure proposed in Figure 1, the corresponding transmittance matrix can be written as follows:

$$M = (M_A M_B)^{\frac{N}{2}} M_D (M_B M_A)^{\frac{N}{2}} \tag{15}$$

where

$$M_D = M_{D_1}\cdot M_{D_2}\cdot M_{D_1} \tag{16}$$

$M_A$, $M_B$, and $M_D$ are the characteristic matrices of layers $A$, $B$, and defect region $D$ (for three defect layers $D_1$, $D_2$, $D_1$).

The total transmission coefficient $t$ of the multilayer structure is given by:

$$t = \frac{2q_0}{(M_{11} + q_t M_{12})q_0 + (M_{21} + q_t M_{22})} \tag{17}$$

where $q_0$ and $q_t$ are entities relating to the first and last mediums of the structure. They are given, for TE and TM polarized waves, by:

$$q_0 = \begin{cases} n_0 \cos\theta_0 & \text{for TE mode} \\ \dfrac{\cos\theta_0}{n_0} & \text{for TM mode} \end{cases} \tag{18}$$

$$q_t = \begin{cases} n_t \cos\theta_t & \text{for TE mode} \\ \dfrac{\cos\theta_t}{n_t} & \text{for TM mode} \end{cases} \tag{19}$$

with $n_t$ and $\theta_t$ being the refractive index and ray angle inside the last medium.

The transmittance spectrum $T$ is obtained by using the expression:

$$T = \frac{q_t}{q_0} |t|^2 \tag{20}$$

The electromagnetic properties of a material are estimated by its relative permittivity and permeability. For a metamaterial, these parameters are complex and are expressed, in the microwave band, by [16–18]:

$$\epsilon_A(f) = 1 + \frac{5^2}{0.9^2 - f^2 - if\gamma_e} + \frac{10^2}{11.5^2 - f^2 - if\gamma_e} \tag{21}$$

$$\mu_A(f) = 1 + \frac{3^2}{0.902^2 - f^2 - if\gamma_m} \tag{22}$$

The frequency $f$ is measured in GHz. $\gamma_e$ and $\gamma_m$ are also measured in GHz, and they represent the electric and magnetic damping frequencies; they are also called electric and magnetic loss factors. For a certain frequency band, $\epsilon_A$ and $\mu_A$ are simultaneously negative, and the refractive index is also negative, which is written as [37]:

$$n_A = -\sqrt{|\epsilon_A|\,|\mu_A|} \tag{23}$$

## 3. NUMERICAL CALCULATION AND DISCUSSION

The mathematical model is implemented in MATLAB, and the obtained results are presented in terms of the transmission spectra. All numerical simulations are done with an incidence angle $\theta_0 = 0$. In this case, transmission spectra for TE and TM modes adopt similar frequency behaviors.

First, an observation of the frequency behavior of the permittivity $\epsilon_A$ and the permeability $\mu_A$ of the metamaterial (Eqs. (21) and (22)), in 1 to 6 GHz frequency band, is necessary for a better interpretation of the results of the rest of the work. The electric and magnetic damping frequencies tested are 0 Hz, 0.2 MHz, and 2 MHz; the study is limited to the case $\gamma_e = \gamma_m$. As shown in Figure 2, the electromagnetic properties of the metamaterial change from one frequency band to another: the real parts of $\epsilon_A$ and $\mu_A$ are both negative ($\epsilon_A < 0$ and $\mu_A < 0$) for frequencies below 3.13265 GHz, which corresponds to a DNG material, $\epsilon_A < 0$ and $\mu_A > 0$ from 3.13265 GHz to 3.78655 GHz (which corresponds to epsilon-negative (ENG) material), and $\epsilon_A > 0$, $\mu_A > 0$ for frequency up to 3.78655 GHz (DPS material). Note that, for the three proposed damping frequencies values, the curves plotted for the real parts of $\epsilon_A$ and $\mu_A$ are superimposed. The imaginary parts of $\epsilon_A$ and $\mu_A$ present a variation that decreases towards zero, without canceling, when the frequency increases except for the case $\gamma_e = \gamma_m = 0$ Hz where the imaginary part is completely zero. For $\gamma_e = \gamma_m = 0.2$ MHz, the imaginary parts of $\epsilon_A$ and $\mu_A$ are less than or equal 0.001 for frequencies 1.9925 GHz and 1.58135 GHz, respectively.

To validate our numerical codes, an initial 1DMPC structure, given in [38], is reproduced. It is composed of alternating layers of metamaterial and silicon (Si) and only one defect layer ($N_d = 1$), such

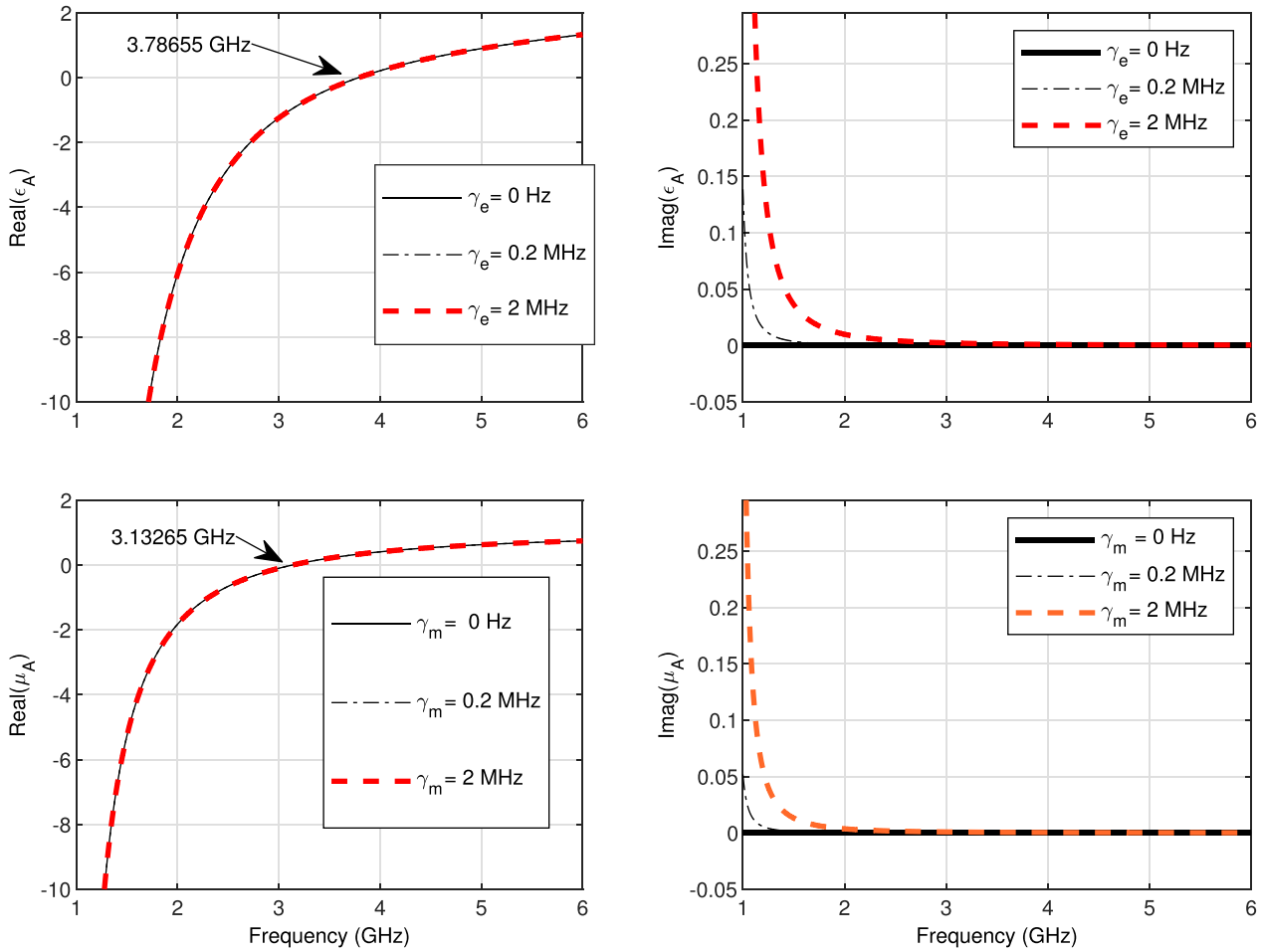


**Figure 2.** Variation of $\epsilon_A$ and $\mu_A$ of the metametrial versus frequency and according to the damping frequencies $\gamma_e$ and $\gamma_m$.

as $M_D = M_{D_1}$ (Eq. (16)), and operating in the range 3.15 to 4.5 GHz. In this frequency interval, the metamaterial is not DNG. The thickness of the latter and that of Si are $d_A = 31.5$ mm and $d_B = 9$ mm, respectively. The refractive index of Si is $n_B = 3.46$ [38]. The defect layer is a dielectric material of positive refractive index $n_{f_1} = \sqrt{\epsilon_{f_1}}$ and thickness $d_{f_1} = 15$ mm. The periodicity number $N$ is equal to 6.

In Figure 3, the transmission spectrum is plotted against the frequency for different values of the defect layer permittivity ($\epsilon_{f_1} = 2.5$, 4, and 6) and according to different values of the damping frequencies (only the case of lossless metamaterial, $\gamma_e = \gamma_m = 0$ Hz, was treated in [38]). As expected, the introduced defect layer caused a peak of transmission in the PBG. A defect mode is detected around 4.0256 GHz, 3.77316 GHz, and 3.55962 GHz when $\epsilon_{f_1}$ is equal to 2.5, 4, and 6, respectively, in a PBG estimated between 3.2928 GHz and 4.2191 GHz. As observed, the defect peak frequency shifts towards lower frequencies as the permittivity, and consequently the refractive index $n_{f_1}$ of the defect layer increases. Results are similar to those of [38] for the case of lossless metamaterial. The effects of the magnetic and electric damping frequencies, which correspond to the lossy metamaterial layers, are examined in terms of transmission efficiency and quality factor of the related defect mode. Note that the peak frequency remains unchanged when the loss factors change. Table 1 gives parameters for the defect peaks according to the permittivity of the defect layer tested and according to the damping frequencies. The loaded quality factor $Q$ and unloaded quality factor $Q_u$ are quantities that can be

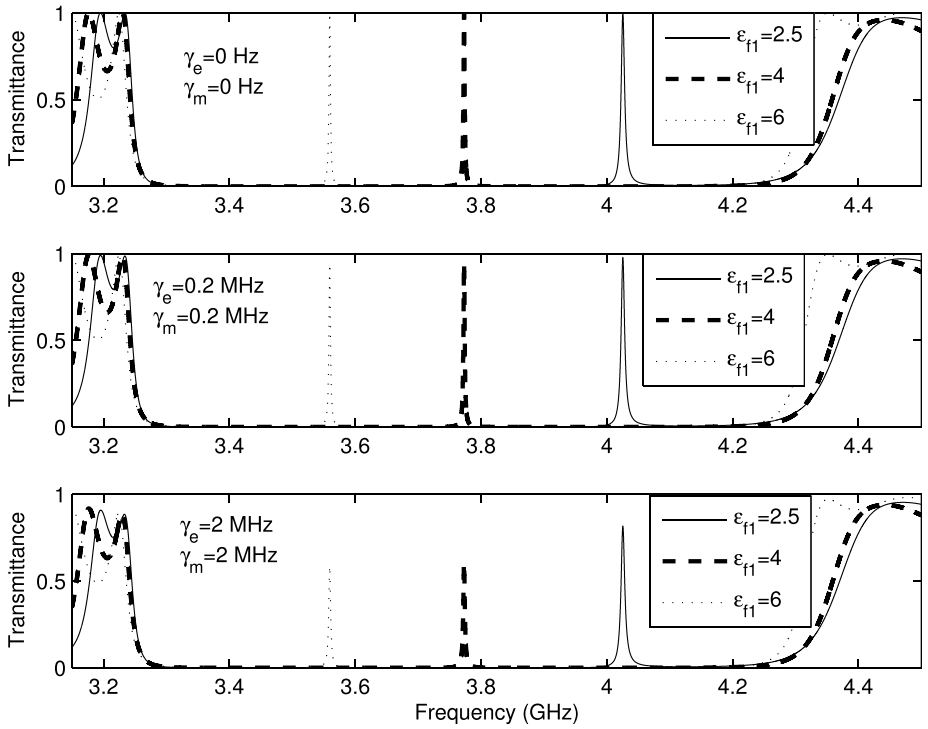


**Figure 3.** Transmission spectra of symmetric 1DMPC with one ($N_d = 1$) defect layer of permittivity $\epsilon_{f1} = 2.5$, 4 and 6, in the band 3.15 to 4.5 GHz, and according to some values of $\gamma_e$ and $\gamma_m$ (with $d_A = 31.5\,\text{mm}$, $d_B = 9\,\text{mm}$, $d_{f_1} = 15\,\text{mm}$, $N = 6$).

given by [39, 40]:

$$Q = \frac{f_{\text{peak}}}{BW_{\text{peak}}} \tag{24}$$

$$Q_u = \frac{Q}{1 - T_{\text{peak}}} \tag{25}$$

where $f_{\text{peak}}$ and $BW_{\text{peak}}$ are the peak frequency and full width at $-3\,\text{dB}$ of the defect mode, respectively. $T_{\text{peak}}$ reflects the amplitude of the transmission coefficient at $f_{\text{peak}}$; it represents the transmittance intensity of the defect mode. High quality factor and transmittance intensity reflect low attenuation losses for a defect mode in the PBG.

As can be seen, the intensity $T_{\text{peak}}$ of the defect peak is affected by the loss factors of the metamaterial; a similar finding has already been given in [41] by Aghajamali et al. $T_{\text{peak}}$ decreases while $BW_{\text{peak}}$ increases with increasing values of the loss factor, whether electric or magnetic. Therefore, the quality factor is also affected as the loss factor increases.

In the goal to explore the frequency interval where the metamaterial is DNG, the same defect configuration ($N_d = 1$) is used with a defect layer permittivity $\epsilon_{f_1} = 4$. The configuration and thicknesses of the periodic layers (DNG/Si) remain unchanged, but the total number of periods was changed to $N = 10$ in order to achieve satisfactory results in terms of detection of defect peaks and performance in the PBG. Increasing the number of periods (or layers) improved the reflectivity of the band gap and made its edges steeper. Let's call this configuration 1D-DNG-PC. Figure 4 shows the transmission spectra, in the band 1.5 to 2.2 GHz, for different values of the defect layer thickness ($d_{f_1} = 1\,\text{mm}$, 4 mm and 7 mm) and according to $\gamma_e = \gamma_m = 0\,\text{Hz}$ and $\gamma_e = \gamma_m = 0.2\,\text{MHz}$. The 1D-DNG-PC structure exhibits two PBGs with appearance of defect modes when the defect layer is introduced. The first PBG (or PBG1) is estimated from 1.565298 GHz to 1.676457 GHz, and the second one (or PBG2) is from 1.883631 GHz to 2.100051 GHz. The defect peak shifts to lower frequencies when the defect layer thickness increases, and as it is predicted, the intensity of the peak decreases with increasing values of

**Table 1.** Defect mode parameters for lossy 1DMPC ($N = 6$, $N_d = 1$, $d_A = 31.5\,\text{mm}$, $d_B = 9\,\text{mm}$, $d_{f_1} = 15\,\text{mm}$).

| $\epsilon_{f_1}$ | $\gamma_e = \gamma_m$ (MHz) | $f_{\text{peak}}$ (GHz) | $T_{\text{peak}}$ | $BW_{\text{peak}}$ (MHz) | $Q$ | $Q_u$ |
|---|---|---|---|---|---|---|
| 2.5 | 0 | 4.0255955 | 0.9999999997 | 4.142 | 971.9 | $3.24 \times 10^{12}$ |
| | 0.2 | 4.0255975 | 0.979242 | 4.1838 | 962.187 | 46352.6 |
| | 2 | 4.0256175 | 0.8179 | 4.5663 | 881.6 | 4841.26 |
| 4 | 0 | 3.7731595 | 0.9999999875 | 1.519 | 2484 | $1.99 \times 10^{11}$ |
| | 0.2 | 3.77316 | 0.945746 | 1.561 | 2417.14 | 44552.34 |
| | 2 | 3.773162 | 0.607113 | 1.945 | 1939.93 | 4937.63 |
| 6 | 0 | 3.5596235 | 0.9999999899 | 1.7578 | 2025 | $2 \times 10^{11}$ |
| | 0.2 | 3.559623 | 0.9415765 | 1.811 | 1965.56 | 33643.25 |
| | 2 | 3.5596175 | 0.5861655 | 2.2913 | 1553.5 | 3754 |

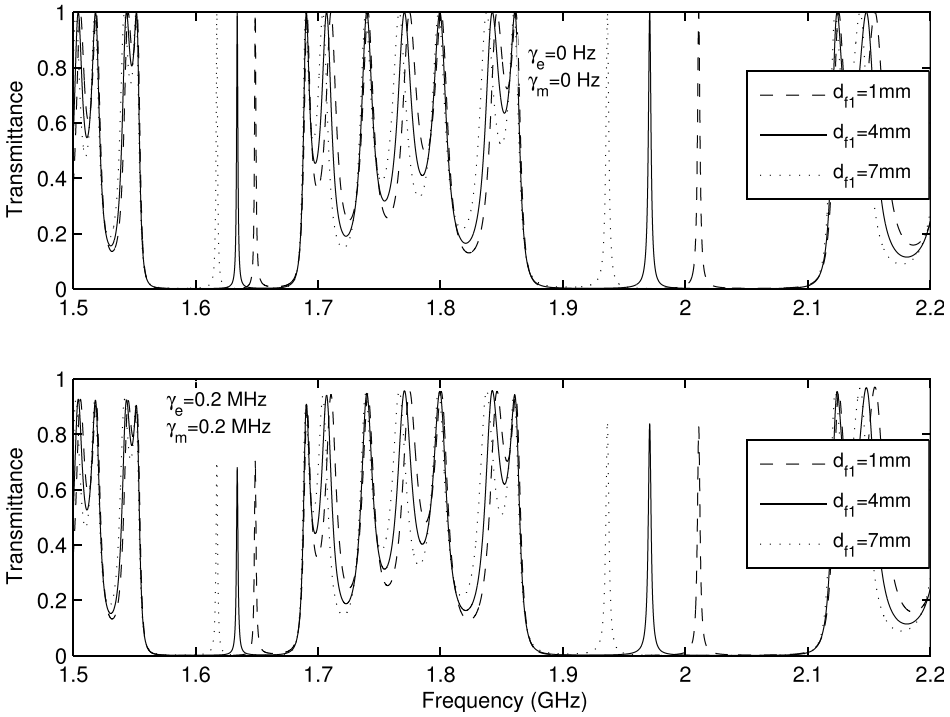


**Figure 4.** Transmission spectra of 1D-DNG-PC with one ($N_d = 1$) defect layer of permittivity $\epsilon_{f1} = 4$ and different thicknesses $d_{f_1}$, and according to $\gamma_e = \gamma_m = 0\,\text{Hz}$ and $\gamma_e = \gamma_m = 0.2\,\text{MHz}$ (with $d_A = 31.5\,\text{mm}$, $d_B = 9\,\text{mm}$, $N = 10$).

$\gamma_e$ and $\gamma_m$.

With these relatively small thicknesses of the defect layer, it was found that a very low frequency shift on the defect peak was observed in the variation of the defect peak frequency, according to the variation of the permittivity $\epsilon_{f_1}$ of the defect material. This frequency shift would be considerably greater when fairly large values of the defect layer thickness would be assigned. But this proposal remains an unconvincing choice because the targeted objective of detecting defect peaks in both PBGs and keeping a correct frequency shift, when the values of the permittivity $\epsilon_{f_1}$ increase, has proved difficult to achieve. Controling the peak frequency in the two PBGs, without changing the whole configuration of the structure, is not feasible.

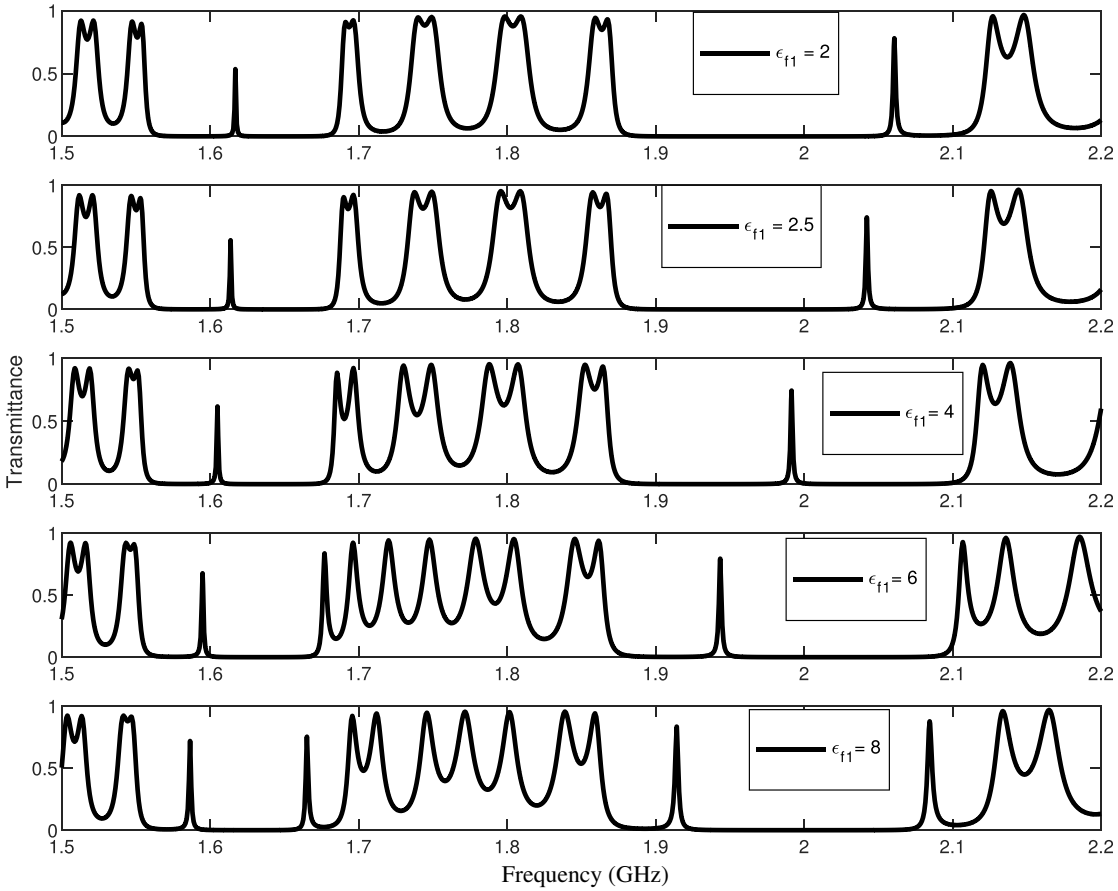


**Figure 5.** Transmission spectra of 1D-DNG-PC with three ($N_d = 3$) defect layers, according to different values of defect layer permittivity (with $d_A = 31.5\,\text{mm}$, $d_B = 9\,\text{mm}$, $d_{f_1} = 18.5\,\text{mm}$, $d_{f_2} = 20.3\,\text{mm}$, $N = 10$, $\gamma_e = \gamma_m = 0.2\,\text{MHz}$).

To improve the performances which are: allow an acceptable frequency shift and achieve a better peak detection in both PBG1 and PBG2 when a variation on $\epsilon_{f_1}$ is applied, and a layer of metamaterial of thickness $d_{f_2} = 20.3\,\text{mm}$ is introduced in the defect region, as represented in Figure 1. It is placed between two layers of defect dielectric material, with a thickness $d_{f_1} = 18.5\,\text{mm}$ each. Periodicity is still achieved with DNG/Si layers. A satisfactory result is obtained for the two studied PBGs as reported in Figure 5. The PBGs are estimated between 1.5636 GHz and 1.67527 GHz for PBG1 and between 1.88193 GHz and 2.09935 GHz for PBG2, in the case of $\epsilon_{f_1} = 4$. The defect peak shifts appreciably to lower frequencies as $\epsilon_{f_1}$ increases. The possibility of presence of a second peak is observed for $\epsilon_{f_1} = 8$.

A quantitative analysis on the variation of the defect peak frequency as a function of defect layer permittivity $\epsilon_{f_1}$ is done for PBG1 and PBG2, and a curve fitting is exerted to extract the expressions of $\epsilon_{f_1}$ as:

$$\epsilon_{f_1(\text{PBG1})} = 1752.90824 f_{\text{peak}}^2 - 5812.199704 f_{\text{peak}} + 4817.012554 \tag{26}$$

$$\epsilon_{f_1(\text{PBG2})} = -1193.3626509 f_{\text{peak}}^3 + 7262.57589 f_{\text{peak}}^2 - 14761.332765 f_{\text{peak}} + 10023.0276145 \tag{27}$$

$f_{\text{peak}}$ is given in GHz. The corresponding curves are plotted in Figure 6. The expressions (26) and (27) allow calculating the permittivity, in function of a measured defect peak frequency, for a dielectric material placed in the defect region of the proposed 1D-DNG-PC structure. For a dielectric material with an unknown permittivity, it would be easy to estimate the latter when a transmission peak is detected in the PBG.

In Tables 2 and 3, parameters corresponding to the defect peak are reported according to the variation of the permittivity of the defect layer tested, in PBG1 and PBG2, respectively. These

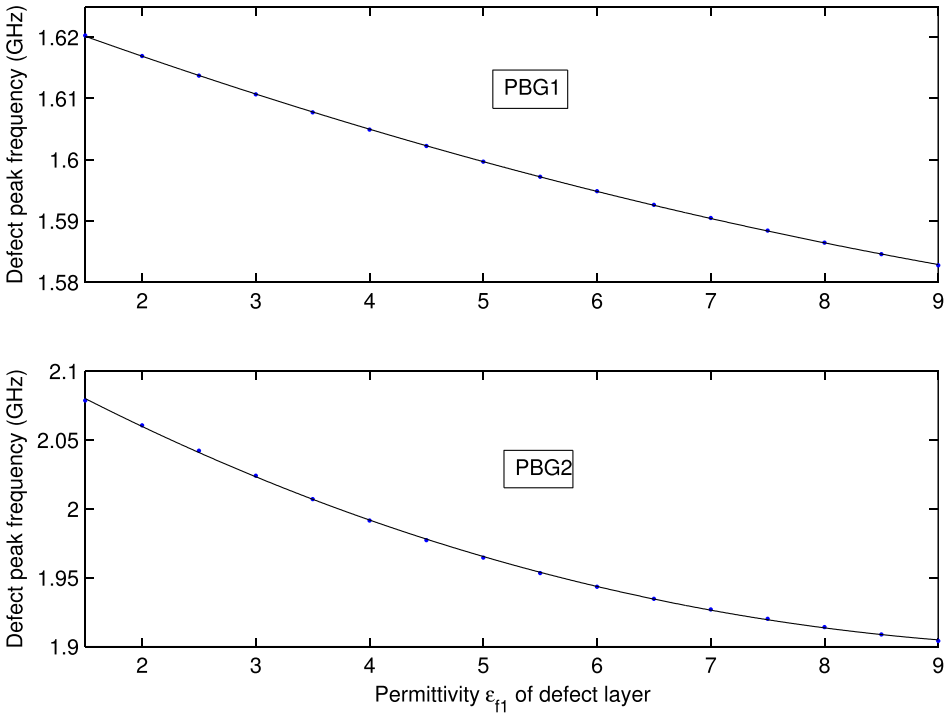


**Figure 6.** Defect peak frequency as a function of defect layer permittivity $\epsilon_{f1}$ for 1D-DNG-PC with three ($N_d = 3$) defect layers in PBG1 and PBG2 ($d_A = 31.5\,\text{mm}$, $d_B = 9\,\text{mm}$, $d_{f_1} = 18.5\,\text{mm}$, $d_{f_2} = 20.3\,\text{mm}$, $N = 10$, $\gamma_e = \gamma_m = 0.2\,\text{MHz}$).

**Table 2.** Defect peak parameters for lossy 1D-DNG-PC in PBG1 ($N = 10$, $N_d = 3$, $d_A = 31.5\,\text{mm}$, $d_B = 9\,\text{mm}$, $d_{f_1} = 18.5\,\text{mm}$, $d_{f_2} = 20.3\,\text{mm}$, $\gamma_e = \gamma_m = 0.2\,\text{MHz}$).

| $\epsilon_{f_1}$ | 2 | 2.5 | 4 | 6 | 8 |
|---|---|---|---|---|---|
| $f_{\text{peak}}$ (GHz) | 1.61696065 | 1.61375295 | 1.60492905 | 1.59488015 | 1.58646385 |
| $T_{\text{peak}}$ | 0.534443227 | 0.557203656 | 0.617393809 | 0.675970645 | 0.71842592 |
| $BW_{\text{peak}}$ (MHz) | 0.60415 | 0.63895 | 0.75223 | 0.9057 | 1.06155 |
| $Q$ | 2676.42 | 2525.63 | 2133.56 | 1760.9 | 1494.48 |
| $Q_u$ | 5748.86 | 5703.8 | 5576.39 | 5434.5 | 5307.6 |

**Table 3.** Defect peak parameters for lossy 1D-DNG-PC in PBG2 ($N = 10$, $N_d = 3$, $d_A = 31.5\,\text{mm}$, $d_B = 9\,\text{mm}$, $d_{f_1} = 18.5\,\text{mm}$, $d_{f_2} = 20.3\,\text{mm}$, $\gamma_e = \gamma_m = 0.2\,\text{MHz}$).

| $\epsilon_{f_1}$ | 2 | 2.5 | 4 | 6 | 8 |
|---|---|---|---|---|---|
| $f_{\text{peak}}$ (GHz) | 2.0607536 | 2.0422224 | 1.9915447 | 1.9434884 | 1.9141869 |
| $T_{\text{peak}}$ | 0.77982788 | 0.741458161 | 0.743475394 | 0.793739991 | 0.83448763 |
| $BW_{\text{peak}}$ (MHz) | 1.27789 | 1.046 | 1.01002 | 1.28075 | 1.68018 |
| $Q$ | 1612.62 | 1952.41 | 1971.79 | 1517.46 | 1139.27 |
| $Q_u$ | 7324.37 | 7551.62 | 7686.54 | 7357.03 | 6883.32 |

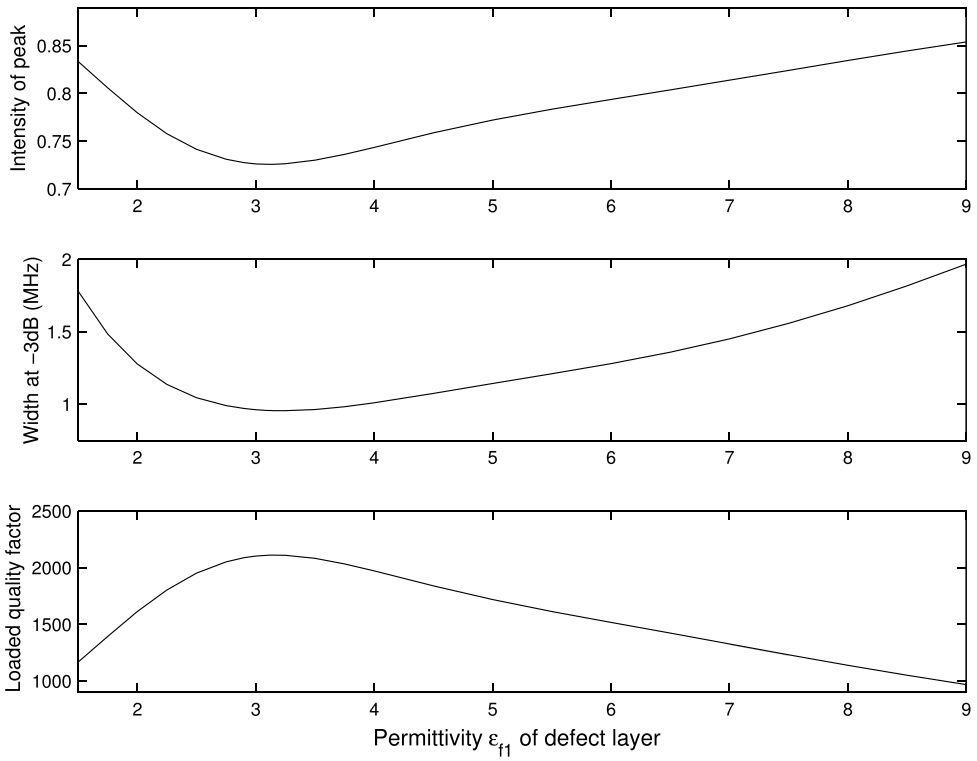


**Figure 7.** Variations of intensity of the peak, width at $-3$ dB and loaded quality factor of the defective 1D-DNG-PC, in PBG2, according to $\epsilon_{f1}$ of defect layer ($D_1$) (with $d_A = 31.5$ mm, $d_B = 9$ mm, $d_{f_1} = 18.5$ mm, $d_{f_2} = 20.3$ mm, $N = 10$, $N_d = 3$, $\gamma_e = \gamma_m = 0.2$ MHz).

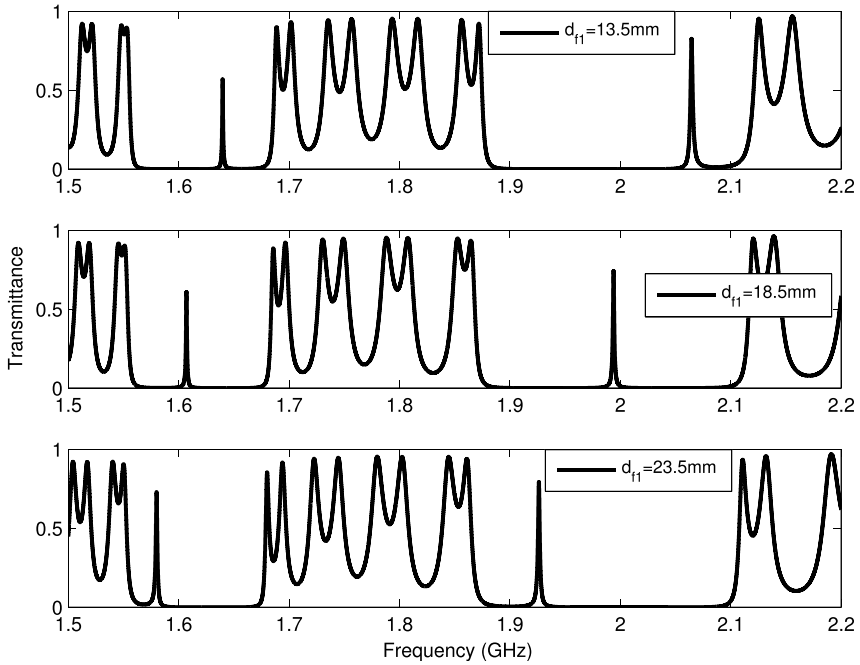


**Figure 8.** Transmission spectra of of 1D-DNG-PC with $N_d = 3$ defect layers, according to the thickness $d_{f_1}$ of defect layer ($D_1$) ($d_A = 31.5$ mm, $d_B = 9$ mm, $d_{f_2} = 20.3$ mm, $\epsilon_{f1} = 4$, $N = 10$, $\gamma_e = \gamma_m = 0.2$ MHz).

parameters are the defect peak frequency, transmittance intensity, bandwidth at −3 dB, loaded and unloaded quality factors. They are also plotted in Figure 7 for PBG2. Contrary to the case seen in the first part of this work (Figure 3 and Table 1), the intensity of the defect peak increases with increasing values of $\epsilon_{f_1}$. An exception is noted, in PBG2, for $\epsilon_{f_1}$ values below 3 (and peak frequency above 2.024168 GHz) where the behavior is rather decreasing. The quality factor decreases with increasing value of $\epsilon_{f_1}$, except also for $\epsilon_{f_1}$ around 3, in PBG2, where it passes through a maximum, as shown in the Figure 7.

To complete the study for the proposed 1D-DNG-PC structure, transmission spectra are also plotted for variations according to the defect layer thickness $d_{f_1}$ of the dielectric material (in Figure 8) and according to the thickness $d_{f_2}$ of the DNG defect layer (in Figure 9). As seen in Figure 8, the defect peak shifts to lower frequencies when $d_{f_1}$ increases in both PBG1 and PBG2. Also, it can be observed, in Figure 9, that by setting $d_{f_2}$ to large enough values, more than one peak can be detected in the PBGs. A multichannel filter can be designed and can have application in a wavelength division multiplexing.

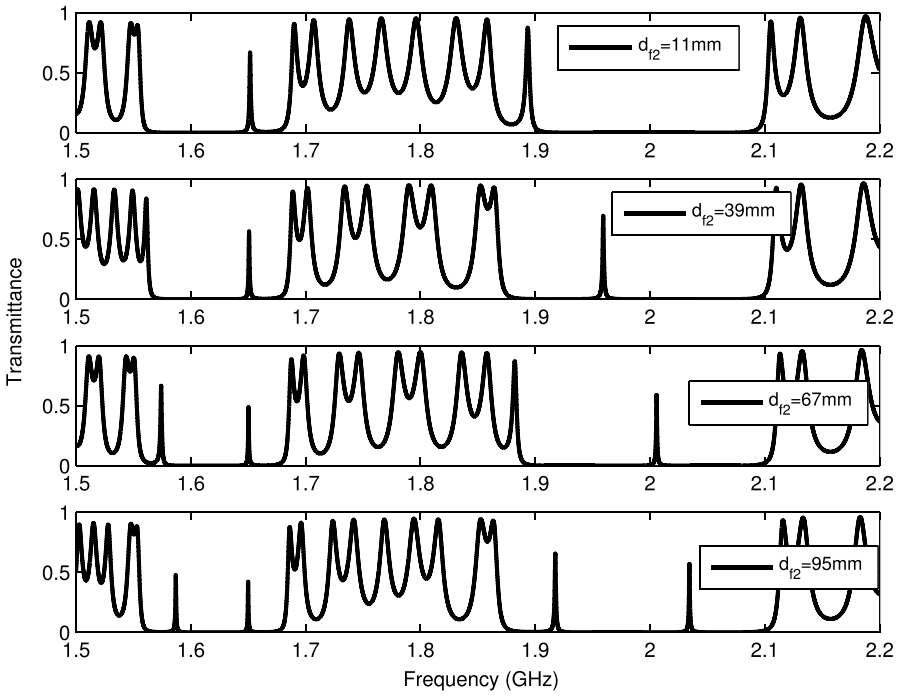


**Figure 9.** Transmission spectra of of 1D-DNG-PC with $N_d = 3$ defect layers, according to the thickness $d_{f_2}$ of DNG defect layer ($D_2$) ($d_A = 31.5$ mm, $d_B = 9$ mm, $d_{f_1} = 18.5$ mm, $\epsilon_{f1} = 4$, $N = 10$, $\gamma_e = \gamma_m = 0.2$ MHz).

## 4. CONCLUSION

In this work, the analysis of symmetric one-dimensional metamaterial photonic crystal (1DMPC) is investigated using the transfer matrix method. The structure is composed of alternating layers of lossy metamaterial and silicon, arranged periodically. The initial incidence of the electromagnetic wave is assumed normal. Defect layers are introduced in the middle of the structure to ensure the generation of defect mode (or transmission mode) in the photonic band gap (PBG) and consequently achieve good performance in terms of tuning its peak frequency when the permittivity or thickness of the defect layer varies. In the first part of the study, transmission spectrum plots are established in the band 3.2 to 4.25 GHz for a defective 1DMPC structure with only one dielectric defect layer. As is already known, the metamaterial offers better properties to 1DPC structures when being integrated into them. However, observation of the behavior of transmission peak as a function of the electric and magnetic loss factors, corresponding to the metamaterial, shows that the latter considerably influence the intensity,

the bandwidth at −3 dB, and consequently the quality factor of the defect mode. The quality factor decreases with increasing values of the loss factors. A similar 1DMPC structure is subsequently treated to explore a lower frequency band between 1.5 and 2.2 GHz; the metamaterial is DNG in this band. The defective region is composed of three layers (combination of a dielectric material and a DNG material). With this configuration, two narrower PBGs are investigated, and the detection of transmission modes is ensured in both of them. When loss factors are quite low, narrow transmission modes are observed, with interesting values of the quality factor. On the other hand, by using lossy metamaterial, the intensity, therefore the quality factor of the mode decreases. Note that the quality factor is also affected by increasing values of the permittivity of dielectric defect. Expressions for calculating the permittivity of a dielectric material placed in the defect region, as a function of a measured frequency of the defect peak, are given for the two PBGs studied. This type of structure can be exploited for the design of very narrow band filters.

## REFERENCES


1. Vanbésien, O., *Artificial Material*, Jefferson Digital Commons, 2012.
2. Suthar, B. and G. N. Pandey, "Optical properties of one dimensional ternary metamaterial photonic crystal," *Macromolecular Symposia, Wiley Online Library*, Vol. 397, 2000340-1–2000340-3, 2021.
3. Biswas, R. and N. Mazumder, "Recent advances in plasmonic probes: Theory and practice," *Springer Cham*, 2022, https://doi.org/10.1007/978-3-030-99491-4.
4. Wu, F., G. Lu, Z. Guo, H. Jiang, C. Xue, M. Zheng, C. Chen, G. Du, and H. Chen, "Redshift gaps in one-dimensional photonic crystals containing hyperbolic metamaterials," *Physical Review Applied*, Vol. 10, No. 6, 2018.
5. Shadrivov, I. V., A. A. Sukhorukov, and Y. S. Kivshar, "Complete band gaps in one-dimensional left-handed periodic structures," *Phys. Rev. Lett.*, Vol. 95, No. 19, 193903, 2005.
6. Lee, C. R., S. H. Lin, S. M. Wang, J. D. Lin, Y. S. Chen, M. C. Hsu, J. K. Liu, T. S. Mo, and C. Y. Huang, "Optically controllable photonic crystals and passively tunable terahertz metamaterials using dye-doped liquid crystal cells," *J. Mater. Chem. C*, Vol. 6, No. 18, 4959, 2018.
7. Xi, F. and L. Hu, "Omnidirectional reflectance gaps and resonant tunneling effect in a one-dimensional photonic crystal consisting of two metamaterials," *Eur. Phys. J. D*, Vol. 66, No. 2, 1, 2012.
8. Srivastava, S. K. and A. Aghajamali, "Study of optical reflectance properties in 1D annular photonic crystal containing double negative (DNG) metamaterials," *Physica B: Condensed Matter.*, Vol. 489, 67–72, 2016.
9. Schurig, D., J. J. Mock, B. J. Justice, et al., "Metamaterial electromagnetic cloak at microwave frequencies," *Science*, Vol. 314, No. 5801, 977–980, 2006.
10. Cong, L. Q., S. K. Valiyaveedu, J. H. Shi, and X. Q. Zhang, "Editorial: Terahertz radiation: Materials and applications," *Frontiers in Physics*, Vol. 9, Article 671647, 2021.
11. Isić, G., B. Vasić, D. C. Zografopoulos, R. Beccherelli, and R. Gajić, "Electrically tunable critically coupled terahertz metamaterial absorber based on nematic liquid crystals," *Physical Review Applied*, Vol. 3, Article 064007, 2015.
12. Wu, F., T. Liu, and S. Xiao, "Polarization-sensitive photonic bandgaps in hybrid one-dimensional photonic crystals composed of all-dielectric elliptical metamaterials and isotropic dielectrics," *Applied Optics*, Vol. 62, 706–713, 2023.
13. Smith, D. R., J. B. Pendry, and M. C. K. Wiltshire, "Metamaterials and negative refractive index," *Science*, Vol. 305, 788–792, Aug. 2000.
14. Vynck, K., "Optical properties of nanostructured dielectric materials: From photonic crystals to metamaterials," Université Montpellier II — Sciences et Techniques du Languedoc, 2008.
15. Sabah, C. and S. Uckun, "Multilayer system of Lorentz/Drude type metamaterials with dielectric slabs and its application to electromagnetic filters," *Progress In Electromagnetics Research*, Vol. 91, 349–364, 2009.

16. Veselago, V. G., "The electrodynamics of substances with simultaneously negative values of $\epsilon$ and $\mu$," *Soviet Physics Uspekhi*, Vol. 10, 509–514, 1968.
17. Smith, D. R., W. J. Padilla, D. C. Vier, S. C. Nemat-Nasser, and S. Schultz, "Composite medium with simultaneously negative permeability and permittivity," *Phys. Rev. Lett.*, Vol. 84, 4184–4187, 2000.
18. Shelby, R. A., D. R. Smith, and S. Schultz, "Experimental verification of a negative index of refraction," *Science*, Vol. 292, 77–79, 2001.
19. Cui, T. J. and J. A. Kong, "Time-domain electromagnetic energy in a frequency-dispersive left-handed medium," *Physical Review B*, Vol. 70, 205106, 2004.
20. Jiang, H., H. Chen, H. Li, and Y. Zhang, "Omnidirectional gap and defect mode of one-dimensional photonic crystals containing negative-index materials," *Appl. Phys. Lett.*, Vol. 83, 5386–5388, 2003.
21. Kumar, N., Sonika, B. Suthar, and A. Rostami, "Novel optical behaviors of metamaterial and polymer-based ternary photonic crystal with lossless and lossy features," *Optics Communications*, Vol. 529, 129073, 2023.
22. Ankita, S. Bissa, B. Suthar, and A. Bhargava, "Graded photonic crystal as improved sensor for nanobiophotonic application," *Macromolecular Symposia*, Vol. 401, 1–4, 2022.
23. Suthar, B., N. Kumar, and S. A. Taya, "Design and analysis of tunable multichannel transmission filters with a binary photonic crystal of silver/silicon," *The European Physical Journal Plus*, Vol. 137, 2022.
24. Sakoda, K., *Optical Properties of Photonic Crystals*, Springer Berlin Heidlberg, New York, 2005.
25. Smith, D. R., R. Dalichaouch, N. Kroll, S. Schultz, S. L. McCall, and P. M. Platzman, "Photonic band structure and defect in one and two dimensions," *J. Opt. Soc. Am. B*, Vol. 10, 314–321, 1993.
26. Oraizi, H. and A. Abdolali, "Several theorems for reflection and transmission coefficients of plane wave incidence on planar multilayer metamaterial structures," *IET Microw. Antennas Propag.*, Vol. 4, 1870–1879, 2010.
27. Jen, Y. J., C. C. Lee, K. H. Lu, C. Y. Jheng, and Y. J. Chen, "Fabry-Perot based metal-dielectric multilayered filters and metamaterials," *Optics Express*, Vol. 23, 33028–33017, 2015.
28. Jiang, H., H. Chen, H. Li, Y. Zhang, J. Zi, and S. Zhu, "Properties of one-dimensional photonic crystals containing single-negative materials," *Physical Review E*, Vol. 69, 1–5, 2004.
29. Yeh, P., *Optical Waves in Layered Media*, Wiley, New York, 1988.
30. Barkat, O., "Theoretical investigation of transmission and dispersion properties of one dimensional photonic crystal," *Journal of Electrical and Electronic Engineering*, Vol. 3, No. 2, 12–18, 2015.
31. Pandey, G. N. and B. Suthar, "Transmittance properties of superconductor-dielectric photonic crystal," *Materials Today: Proceedings*, Vol. 49, No. 1, 2021.
32. Ankita, S. Bissa, B. Suthar, C. Nayak, and A. Bhargava, "An improved optical biosensor design using defect/metal multilayer photonic crystal for malaria diagnosis," *Results in Optics*, Vol. 9, 2022.
33. Cheng, D. K., *Field and Wave Electromagnetics*, Addison-Wesley Publishing Company, New York, 1989.
34. Srivastava, S. K. and A. Aghajamali, "Narrow transmission mode in one-dimensional symmetric defective photonic crystal containing metamaterial and high Tc superconductor," *Optica Applicata*, Vol. 49, No. 1, 2019.
35. Chettah, C., O. Barkat, and A. Chaabi, "Tunable properties of optical selective filters based on one-dimensional plasma superconductor photonic crystal," *Journal of Super-conductivity and Novel Magnetism*, Vol. 34, 2239–2248, 2021.
36. Thabet, R. and O. Barkat, "Transmission spectra in one-dimensional defective photonic crystal integrating metamaterial and superconductor," *Journal of Super-conductivity and Novel Magnetism*, Vol. 35, 1473–1482, 2022.
37. Pendry, J. B., "Negative refraction makes a perfect lens," *Phys. Rev. Lett.*, Vol. 85, No. 18, 3966–3969, 2000.

38. Aly, A. H., A. A. Ameen, M. A. Mahmoud, Z. S. Matar, M. Al-Dossari, and H. A. Elsayed, "Photonic crystal enhanced by metamaterial for measuring electric permittivity in GHz range," *Photonics*, Vol. 8, 416, 2021.
39. Pozar, D. M., *Microwave Engineering*, Addison-Wesley Publishing Company, New York, 1990.
40. Park, J. H. and J. G. Park, "Uncertainty analysis of $Q$ factor measurement in cavity resonator method by electromagnetic simulation," *SN Applied Sciences*, Vol. 2, 996, 2020, https://doi.org/10.1007/s42452-020-2819-8.
41. Aghajamali, A., T. Alamfard, and M. Hayati, "Loss factor dependence of defect mode in a 1D defective lossy photonic crystal containing DNG materials," *Optik — International Journal for Light and Electron Optics*, 2015.